



OPEN

SUBJECT AREAS:
ELECTRONIC PROPERTIES
AND DEVICES
ELECTRONIC MATERIALSReceived
17 March 2014Accepted
4 April 2014Published
28 April 2014Correspondence and
requests for materials
should be addressed to
W.H.T. (whtang@mail.
njust.edu.cn)

MnO₂ Nanorods Intercalating Graphene Oxide/Polyaniline Ternary Composites for Robust High-Performance Supercapacitors

Guangqiang Han¹, Yun Liu¹, Lingling Zhang¹, Erjun Kan², Shaopeng Zhang¹, Jian Tang¹ & Weihua Tang¹¹Key Laboratory of Soft Chemistry and Functional Materials (Ministry of Education of China), Nanjing University of Science and Technology, Nanjing 210094, People's Republic of China, ²Department of Applied Physics, Nanjing University of Science and Technology, Nanjing 210094, P. R. China.

New ternary composites of MnO₂ nanorods, polyaniline (PANI) and graphene oxide (GO) have been prepared by a two-step process. The 100 nm-long MnO₂ nanorods with a diameter ~20 nm are conformably coated with PANI layers and fastened between GO layers. The MnO₂ nanorods incorporated ternary composites electrode exhibits significantly increased specific capacitance than PANI/GO binary composite in supercapacitors. The ternary composite with 70% MnO₂ exhibits a highest specific capacitance reaching 512 F/g and outstanding cycling performance, with ~97% capacitance retained over 5000 cycles. The ternary composite approach offers an effective solution to enhance the device performance of metal-oxide based supercapacitors for long cycling applications.

Supercapacitor or electrochemical capacitors, featuring high power density, long cycle life, fast charge and discharge rates^{1–7}, have attracted tremendous attention in energy storage. During the last decades, different kinds of materials have been studied as possible supercapacitor electrodes, namely, carbonaceous materials, conducting polymers and transition metal oxides^{8–11}. Among them, transition-metal oxides such as RuO₂^{12–13}, NiO^{14,15} and MnO₂^{16–20}, are the most widely used electrode materials thanks to their large capacitance, high surface area and relatively good electrical conductivity. Compared to other transition-metal oxides, MnO₂ is generally regarded as the most promising one for the next generation of supercapacitors because of its ideal capacitor performances, good cycle stability, low cost and environmental friendliness^{21,22}. However, the poor electrical conductivity and densely packed structure limit its application in the development of high-performance supercapacitors²³. For this purpose, some efforts have been made to develop nanostructured MnO₂/carbonaceous materials (ca. graphene, carbon nanotube or carbon nanofibers) based binary composites^{24,25} or their ternary composites with conducting polymers^{26–31}. The carbonaceous materials or conductive polymers act as not only 3-dimensional (3-D) scaffold but conductive wrappings to enhance the specific capacitance and cycle stability of the electrodes fabricated with these composites. Our recent studies have shown that conductive polymer coatings prepared via in-situ redox process can greatly improve the conductivity and specific area of the resulted composites^{32,33}.

As one of the most appealing carbon materials, graphene features superior electrical conductivity, excellent mechanical flexibility, and high thermal and chemical stability^{34,35}. Compared with pristine graphene, graphene oxide (GO) has good dispersion in many solvents, particularly in water, and this is important for solution-processing and further derivatization^{36,37}. Though some losses in electrical conductivity when converting from graphite, GO has demonstrated to be a potential substrate to improve the conductivity and stability of MnO₂³⁸. To enhance the performance of MnO₂-graphene composite electrodes, conductive materials were further incorporated to form ternary composites to achieve significantly increased specific capacitance and cycling-stability from the ternary composites based supercapacitors^{26–31}. By depositing 5–10 nm MnO₂/polyaniline (PANI) nanoparticles onto sulfonated graphene nanosheets, the composite (sGMOPANI) based two-electrode cell showed an electrochemical capacitance of 276 F/g at 1 A/g current density³⁰. The ternary composites of graphene/MnO₂ nanostructures with carbon nanotube or poly(3,4-ethylenedioxythiophene):poly(styrenesulfonate) showed ~20% or 45% increased capacitance than graphene/MnO₂ composites, with the highest value as

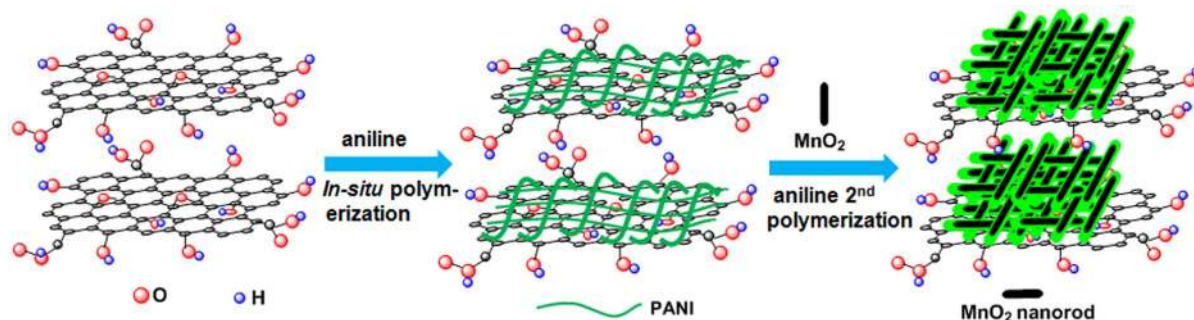


Figure 1 | Illustration for formation of GOPM nanocomposites: (a) *in-situ* polymerization of aniline, (b) dispersion of graphene oxide sheets and MnO₂ nanorods in solution by ultrasonication and self-assembly during the second aniline polymerization.

high as ~ 380 F/g achieved²⁸. The nanostructure of graphene/MnO₂ seems to be important for the performance and stability of the capacitors. Moreover, the overall specific capacitance of MnO₂/carbon composites is generally limited to 250 F/g due to the relatively low weight loading of MnO₂ on carbon surface (usually less than 64 wt.%)²⁵. We were intrigued whether the high loading of MnO₂ nanorods into binary composites of conductive polymers and solution-exfoliated GO nanosheets can improve the electron transport and contribute to the energy storage of the whole composite film to achieve robust high-performance supercapacitors.

We report herein the successful fabrication of graphene oxide-polyaniline-MnO₂ ternary composites, where MnO₂ nanorods were incorporated to intercalate PANI/solution-exfoliated GO nanosheets. MnO₂ nanorods were thus fastened onto GO sheets via PANI layer (Fig. 1). The PANI layer has several advantages: (1) to anchor MnO₂ nanorods onto the surface of GO, (2) to prevent GO sheets and MnO₂ nanorods from stacking/aggregating; (3) to improve the charge transfer between GO and MnO₂ and (4) to prevent MnO₂ from falling off GO sheets during cycling electrochemistry. The composites exhibited greatly improved capacitive performance than GO-MnO₂ and GO-PANI composites. The ternary composites with 70 wt.% MnO₂ delivered a highest specific capacitance of 512 F/g at 0.25 A/g current density, with the capacitive retention of as high as 97% observed after 5100 cycles.

Results

Preparation and characterization of ternary composites. The ternary composites were prepared with a two-step protocol as shown in Fig. 1. After a first step of coating solution-exfoliated GO nanosheets³⁹ with polyaniline, MnO₂ nanorods⁴⁰ were allowed to self-assemble onto the GO sheets and then wrapped by in-situ prepared polyaniline coatings in the second step. The MnO₂ (in weight ratio) content in the ternary composites was determined with thermogravimetric (TGA) analysis (Figure 2). Hence, the as-prepared MnO₂-PANI-GO composites (GOPM) are designated as GOPM-20, GOPM-46 and GOPM-70, meaning that mass percentage of MnO₂ in the composites is about 20%, 46% and 70%, respectively.

Typical X-ray diffraction (XRD) pattern of as-prepared hierarchical porous GOPM-46 and free MnO₂, PANI and GO are shown in Fig. 3a. It can be seen that the XRD pattern of GOPM is similar to those of free MnO₂ and PANI, indicating that the MnO₂ particles have been well immobilized by PANI onto GO substrate. All of the major reflections [$2\theta = 21.2^\circ$ (120), 28.0° (310), 37.5° (131), 42.5° (300), 59.0° (160) and 69.7° (003)] in the XRD pattern can be indexed to the orthorhombic phase of γ -MnO₂ with lattice constants $a = 6.36$ Å, $b = 10.15$ Å and $c = 4.09$ Å (JCPDS 14-644), confirming that γ -MnO₂ crystalline phase forms in the synthesis, which is in good agreement with the reported patterns for γ -MnO₂⁴¹. The broad peak centered at about 25.3° , attributing to the diffraction of (110) plane of the as-formed PANI crystalline phase, suggests the successful

synthesis of PANI. However, the sharp peak at $2\theta = 11.0^\circ$, corresponding to its (002) plane for pure GO⁴², almost disappeared, which is attributed to the increase in inter-space distance of graphene layer due to intercalation of PANI/MnO₂ between GO sheets.

The Raman spectra of GOPM and pristine components are shown in Fig. 3b. It can be clearly seen that both GOPM-46 and MnO₂ samples feature a sharp peak at 640 cm^{-1} , corresponding to the Mn-O vibration perpendicular to the direction of the MnO₆ octahedral double chains of MnO₂⁴³. The Raman-active peaks at 1350 cm^{-1} and 1600 cm^{-1} , corresponding to the in-plane bond-stretching motion of C sp² atoms (G band) and the breathing modes of or of benzenoid rings of GO (D-band), were significantly suppressed in intensity for GOPM-46 sample. The typical peaks for PANI also weakened in GOPM, mainly due to its low content in the hybrid composite.

To confirm the XRD and Raman results, the compositions and the valence states of GOPM were further characterized with XPS and the results are shown in Fig. 3c–f. The peak ~ 284.6 eV (for C 1s) originating from the graphitic sp² carbon atoms and the peak at 531.9 eV corresponding to O1s in C–OH bond are observed for GO (Fig. 3c). The existence of C, N, O, Mn in GOPM can be confirmed from Fig. 3d. For GOPM, the XPS peaks of N 1s (Fig. 3e) are further decomposed into three Gaussian peaks with binding energies of 398.6 (–N=), 399.7 (–NH–) and 400.1 (–N⁺)³⁷. The peak at 400.1 eV is assigned to the quinoid amine and nitrogen cationic radical (N⁺), while the one at 398.6 eV (=N–) is due to benzenoid amine. The Mn 2p spectrum is analyzed in Fig. 3f. Both Mn 2p_{3/2} peak at 643.0 eV and Mn 2p_{1/2} peak centering at 654.5 eV are clearly observed, which are in good agreement with the energy splitting of the standard spectrum of MnO₂⁴⁴. The peak-to-peak separation between Mn 2p_{1/2} and Mn 2p_{3/2} level is 11.5 eV, which is approximately the same value as that literature for MnO₂⁴⁵.

The morphologies of dry MnO₂, GO-PANI and GOPM-46 are observed with FESEM and TEM (Fig. 4,5). Pristine MnO₂ nanorods

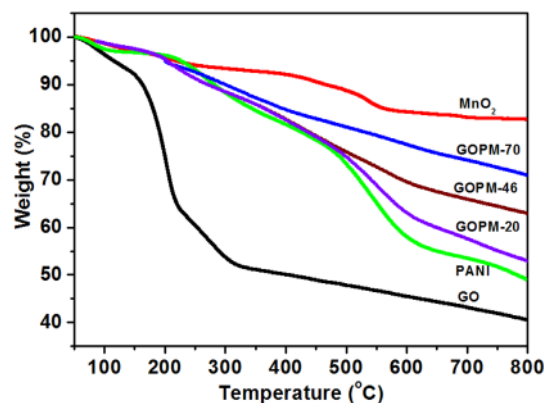


Figure 2 | TGA curves of GO, PANI, MnO₂ and GOPM.

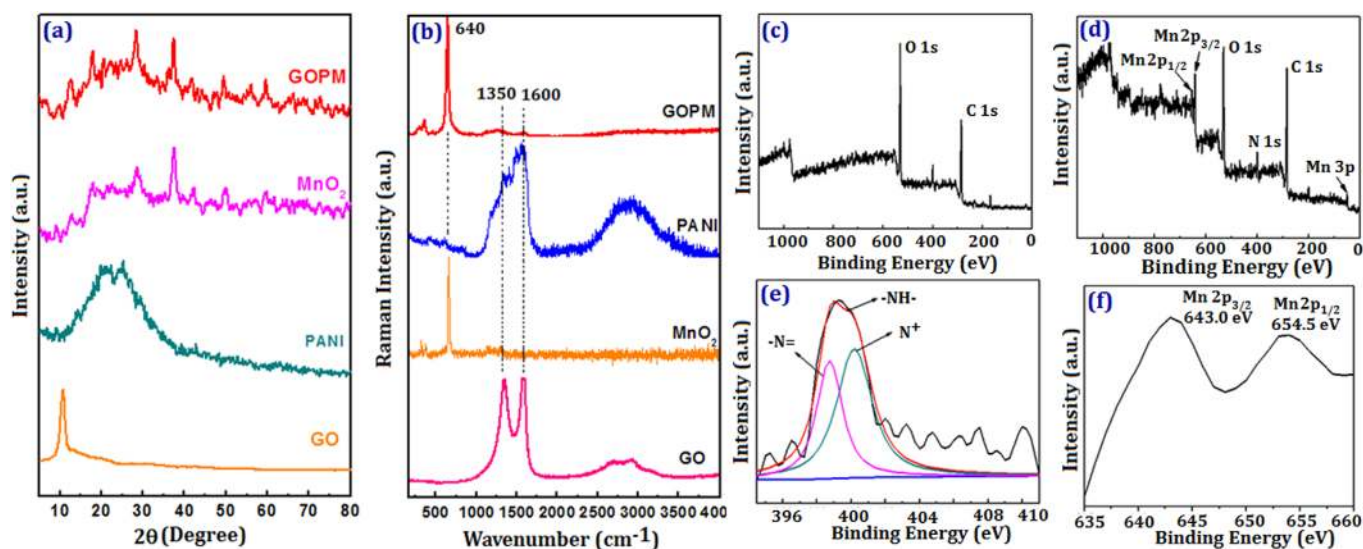


Figure 3 | (a) X-ray diffraction patterns and (b) Raman spectra of GO, MnO₂, PANI, GOPM-46; XPS spectra of (c) GO, (d) GOPM-46 and N 1s in (e) GOPM-46 and (f) Mn 2p in GOPM-46.

with a length of 200 nm grow into nanospheres with diameters ranging from 300 to 600 nm (Fig. 4a). The *in-situ* prepared PANI self-assembled on GO sheets like a broccoli composed numerous of small flower buds with a diameter of 50 nm (Fig. 4b). When MnO₂ nanorods were introduced to GO-PANI system, GOPM hybrid composites feature a porous yet densely packed structure (Fig. 4c), with GO layers intercalated by porous interpenetrating networks of PANI-wrapped MnO₂ nanorods. PANI functions as both protecting coating for MnO₂ nanorods to avoid aggregation and adhesive to fasten GO sheets and MnO₂ nanorods into densely packed structure. Exfoliated GO sheets feature transparent wrinkled tulle in TEM image (Fig. 4d), while PANI formed a compact layer on top of GO sheets for GO-PANI composites.

A close look at the TEM images of GOPM (Fig. 4f and Fig. 5c,d), one would clearly observed the existence of MnO₂ nanorods, featuring a length less than 100 nm and a diameter ~20 nm. With the content of MnO₂ nanorods increasing from 46% to 70% in the composites, the dimensions of MnO₂ nanorods was observed to increase

by 30% (Fig. 5d). Nevertheless, the intimate contact between GO sheets and PANI wrapped MnO₂ nanorods with different lengths can be clearly observed from both SEM and TEM images, which is important for improving electrical conductivity. A close look at the SEM image of ternary composites, GOPM-70 boasts increased porosity than GOPM-46, which can be confirmed by BET measurement. The GOPM-70 and GOPM-46 exhibit a surface area of 91.37 and 73.65 m²/g, respectively, much higher than that for GO-PANI (~36.92 m²/g). The increased surface area can be explained with the constitution of the ternary composites. Since PANI has the equivalent mass with GO, more MnO₂ nanorods were uncovered by PANI with the increase of MnO₂ content. More porous structure was therefore obtained to present higher surface area before heavy aggregation of MnO₂ occurs.

Capacitive performance of ternary composite. The capacitive performance of GO, MnO₂, GO-PANI, GO-MnO₂ and GOPM were evaluated by cycle voltammetry (CV) and galvanostatic

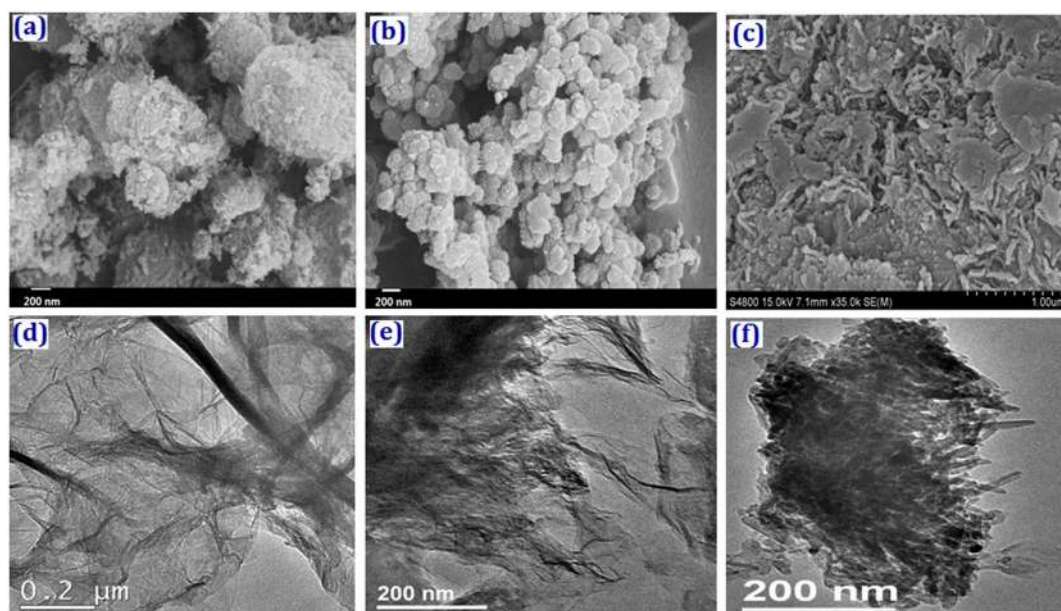


Figure 4 | FE-SEM images of (a) dried pristine MnO₂, (b) GO-PANI and (c) GOPM-46; TEM images of (d) GO sheets, (e) GO-PANI and (f) GOPM-46.

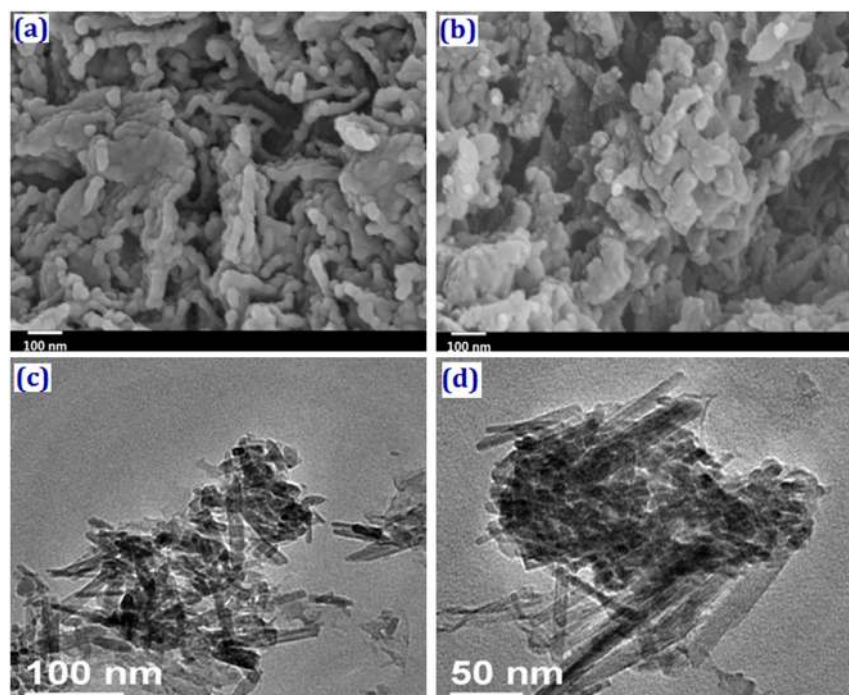


Figure 5 | FE-SEM image of (a) GOPM-46 and (b) GOPM-70, TEM image of (c) GOPM-46 and (d) GOPM-70.

charge/discharge techniques in 1 M Na₂SO₄ solutions. Fig. 6a shows the CV curves of GOPM-46 at different scan rates. At low scan rates (≤ 50 mV/s), GOPM-46 exhibits slight redox peaks, suggesting the pseudocapacitive feature of GOPM. The asymmetrical CV curves can be attributed to the combined double-layer and pseudocapacitive contributions to the total capacitance. The high CV currents indicate the high conductivity and low internal resistance for GOPM as the electrode material. Fig. 6b shows CV curves of GO, MnO₂, GO-PANI, GO-MnO₂ and GOPM at 50 mV s⁻¹, where GOPM-46 exhibits the highest capacitance than other electrodes. This can be attributed to the unique porous structure of hybrid GOPM, which effectively prevent the self-aggregation of GO sheets and MnO₂ nanorods. More importantly, the hybrid GOPM with PANI-coated MnO₂ nanorods intercalated GO nanosheets affords higher surface area to provide better conductive paths for fast electron transportation.

The galvanostatic charge/discharge curves of GOPM in 1 M Na₂SO₄ solution were carried out at a current density of 0.25, 0.5,

1, 2 and 4 A/g. As illustrated in Fig. 7a, all the curves exhibit an equilateral triangle shape, indicating high reversibility of the hybrid materials during charge/discharge process. The charging/discharging process took longer time at lower current density, which is attributed to the sufficient insertion or release of Na⁺ during the charging/discharging process. The specific capacitance (C) of the electrode can be calculated according to equation: $C = It/mV$, where C is the specific capacitance (F/g), I is the charge-discharge current (A), t is the discharge time (s), V is the potential window (V), m is the mass of active material in the working electrode (g)⁴⁶. The galvanostatic charge/discharge curves of MnO₂, GO-MnO₂, GO-PANI, GOPM at 0.25 A/g current density are compared in Fig. 7b. The specific capacitance of GOPM (409 F/g) is much higher than that of MnO₂ (150 F/g), GO-MnO₂ (162 F/g) and GO-PANI (20 F/g) at the same current density. Same trend is observed for GOPM when further increasing current density in the range of 0.25~4 A/g (Fig. 7c), indicating the robustness of the as-prepared hybrid GOPM as electrode materials.

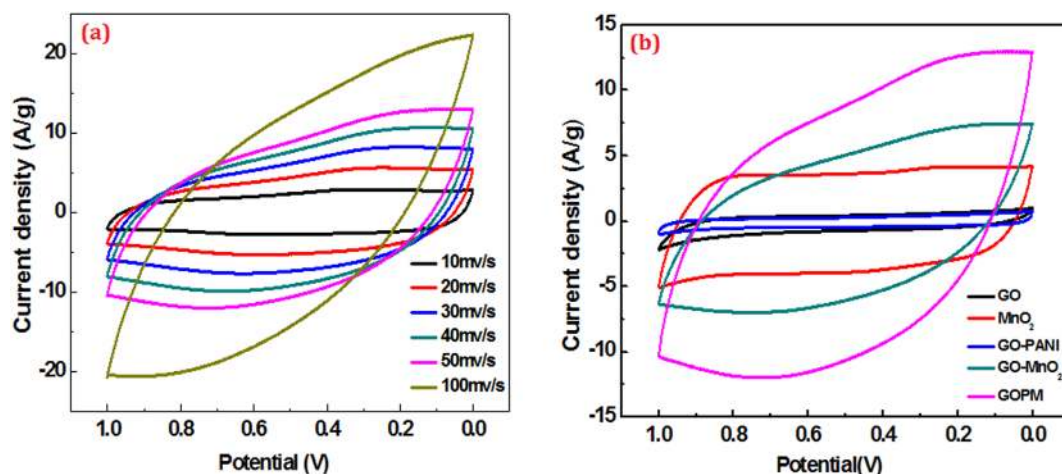


Figure 6 | (a) CV curves of GOPM-46 at scan rate of 10, 20, 30, 40, 50 and 100 mVs⁻¹; (b) CV curves of GO, MnO₂, GO-PANI, GO-MnO₂ and GOPM-46 at scan rate of 50 mV s⁻¹.

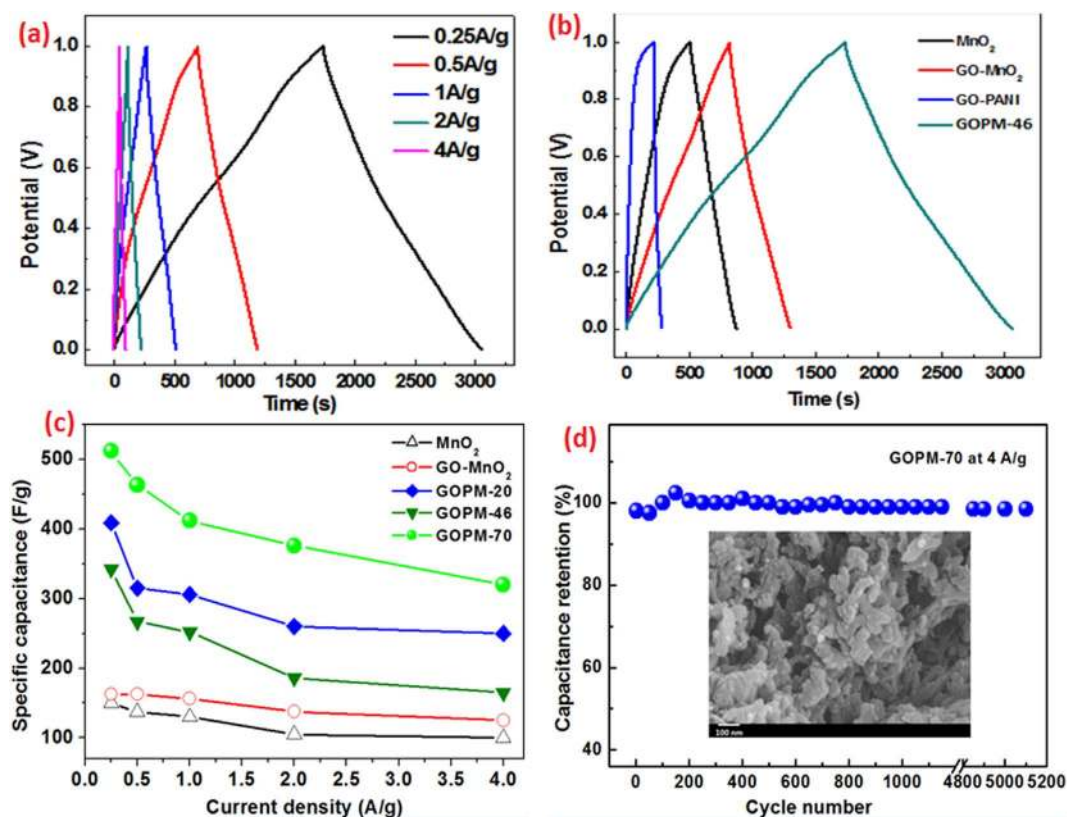


Figure 7 | Galvanostatic charge/discharge curves of (a) GOPM-46 at different current density; (b) MnO_2 , GO-MnO_2 , GO-PANI and GOPM-46 at 0.25 A/g current density; (c) specific capacitance curves of MnO_2 , GO-MnO_2 and GOPM composites at different current densities; (d) capacitance retention of GOPM-70 over cycling times.

The specific capacitance of GOPM is found to increase with the content of MnO_2 in the composite, as shown in Fig. 7c. The specific capacitance of GOPM-70 (412 F/g), GOPM-46 (306 F/g) and GOPM-20 (252 F/g) is about 1~2 times higher than that of MnO_2 (130 F/g) and GO-MnO_2 (156 F/g) at the current density of 1 A/g. Further increase of MnO_2 content over 90%, however, leads to decreased capacitive performance, e.g., the GOPM with 92% MnO_2 delivered a specific capacitance of 382 F/g at 1 A/g current density. The specific capacitance of 412 F/g at 1 A/g for GOPM-70 is much better than graphene/ MnO_2 (78 wt.% MnO_2) binary composite under similar testing conditions²⁵. This improvement may be explained with the contribution of conductive PANI in facilitating charge transport and energy storage. Compared with the ternary composite sGMOPANI^{30} , our composite with MnO_2 nanorods exhibited 11% improved capacitance in supercapacitors at same current density of 1 A/g. The specific capacitance of GOPM decreases with current density, with ~62% capacitance retained for GOPM-70 when the current density increased from 0.25 A/g to 4 A/g.

The electrochemical stability of GOPM-70 nanocomposites was investigated at 4 A/g current density. As shown in Fig. 6d, the capacitance of GOPM electrode retained about 97% of the highest capacitance even after continuous galvanostatic charge/discharge process for 5100 cycles, indicating a good cycling ability of the hybrid composites. The support carbon matrix GO allowed the strong deposition of PANI -protecting MnO_2 nanorods on the surfaces of GO , which enhanced the mechanical strength of composite materials, resulting in the long charge/discharge ability. Interestingly, the specific capacitance showed slight increase in the first 150 cycles before decreased slowly in the later cycles, which may be explained with the insufficient contact of nanocomposites with Na_2SO_4 aqueous solution at the beginning of electrochemical measurement^{39,47}.

The electrochemical properties of GOPM were further evaluated with electrochemical impedance spectroscopy (EIS). The impedance spectra of composite electrodes before and after 3000 cycles were measured in the frequency range of 100 kHz–0.1 Hz at open circuit potential with an AC perturbation of 5 mV (Fig. 8). Theoretically, an ideal Nyquist impedance plot features a semicircle over the high frequency region and a linear part in the low frequency range. The larger semicircle observed for the electrode corresponds to higher interfacial charge-transfer resistance (R_{ct}) for the layer on the electrode, attributed to the poor electrical conductivity of the materials. And the straight line of the Nyquist plot corresponds to the resistance (R_s) resulting from ion diffusion/transport, i.e., the more vertical line is indicative of an electrode more close to an ideal capacitor⁴⁷. The equivalent series resistance (ESR) of pristine MnO_2 , GO-PANI , GOPM-46 and GOPM-70 obtained from the intersection of the Nyquist plot at the x-axis is 2.6, 0.7, 1.8, and 1.6 Ω , respectively. Considering the similar morphology of GO-PANI and GOPM , the difference in ESR of electrodes can be attributed to the different conductivities of electrode materials. The smaller ESR of GOPM than GO-PANI suggests the decreased charge transfer resistance in the presence of MnO_2 nanorods as core⁴⁸. The high resistance of ion transfer in GO-PANI would be attributed to high charge density, resulting in low capacitance. In contrast, GOPM-46 exhibited a short diffusion path length of ions in the electrolyte, which could be seen from the low resistance of the capacitive part on the Nyquist plot. This may be explained by the structure of the composite: the formation of GOPM results in the surface charge of GO being compensated by the negative charge from both Cl^- doped PANI and MnO_2 nanorods, leading to a lower resistance of ion transfer. Moreover, the presence of GO-PANI with high electrical conductivity resulted in a lower charge transfer³⁷. After 3000 cycles, the calculated ESR for

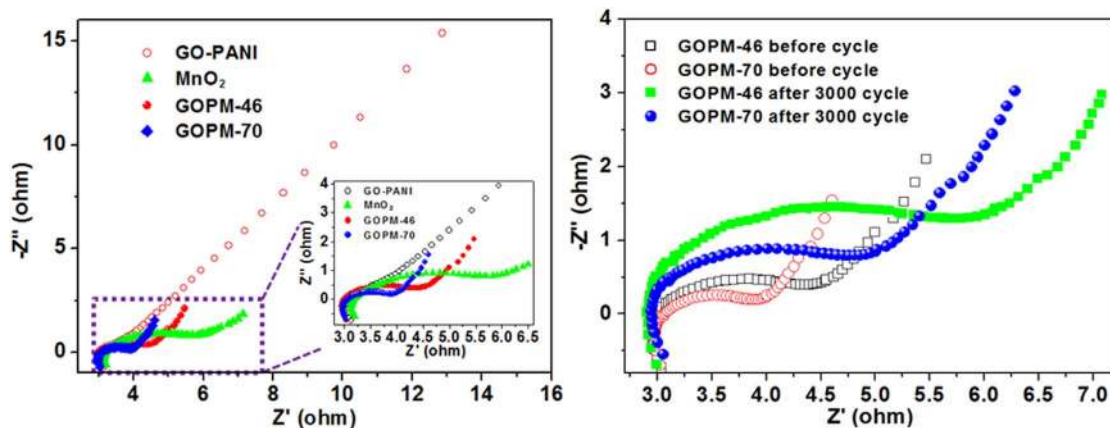


Figure 8 | Nyquist impedance plots of (a) MnO_2 , GO-PANI and GOPM composites before cycle and (b) GOPM after 3000 cycles.

GOPM-46 based electrode increased from 1.8 to 2.4 Ω , while the ESR increased from 1.6 to 2.1 Ω for GOPM-70. The increased resistance is probably attributed to the loss of adhesion of some active material with the current collector or the dissolution of some PANI/ MnO_2 during the charge/discharge cycling.

Discussion

By using a quick and facile two-step process, MnO_2 nanorods were successfully coated by in-situ prepared PANI and intercalated into GO sheets. The as-prepared ternary composites with different loading of MnO_2 were evaluated as electrode materials for supercapacitors. The ternary composites presented highly porous nanostructure with significantly increased surface area (91.37 and 73.65 m^2/g , respectively, for GOPM-70 and GOPM-46). With MnO_2 nanorods to facilitate the charge transport in energy storage application, the ternary composites exhibited increased specific capacitance with the loading of MnO_2 before a maximum reached at 70 wt.% MnO_2 . The GOPM-70 electrode exhibits a highest specific capacitance of 512 F/g at 0.25 A/g current density. With PANI conductive coating, the electrode showed high electrochemical stability in cycling, with $\sim 97\%$ capacitance retention observed after 5100 cycles. Importantly, this design strategy may be employed for the fabrication of robust high-performance electrode with tailor-made hybrid composites composed of carbonaceous materials, conducting polymers and metal oxides.

Methods

Preparation of MnO_2 nanorods⁴⁰. Absorbent cotton (200 mg) was added to KMnO_4 solution (40 mM, 200 mL) with simultaneous vigorous stirring and ultrasonic irradiation for 20 min. The mixture suspension was then heated at 100°C for 24 h. A dark brown precipitate was obtained. The precipitates were collected by centrifugation and washed with deionized water and ethanol for 4 times. The *titile* product was dispersed in hydrochloric acid (1 M) for use.

Preparation of MnO_2 /PANI/GO ternary hybrid nanostructures. Freshly prepared GO (0.1 g) dispersion in water (100 mL)³⁹ was ultrasonicated (250 W, 220 V) for 1 h to get an exfoliated yellow brown GO suspension. Aniline (0.12 g) was slowly added into the suspension and the stable GO/aniline suspension was obtained after stirring violently. A mixture of concentrated hydrochloric acid, ammonium persulfate (APS) in distilled water (10 mL) was then slowly added to the suspension under stirring. The molar ratio of aniline, hydrochloric acid and APS was 1 : 1 : 1. When the reaction was conducted in ice bath for 10 minutes, MnO_2 nanorods (0.6 g) dispersion in hydrochloric acid (1 M, 50 mL) was added to the reaction system together with second addition of aniline (0.12 g). The reaction was stirred for 12 h. Finally, the composite was filtered and rinsed with distilled water and ethanol in sequence to afford the *titile* product (0.65 g) as a deep green solid.

Characterization. Thermogravimetric analysis (TGA) was conducted on a TA instrument TGA/SDTA851 at 20°C/min heating rate under nitrogen. Raman spectra were performed on a Renishaw laser confocal Raman spectrometer employing a 514 nm laser beam. The XRD patterns were recorded on an X-ray diffractometer (D8 Advance, Bruker, Germany) by using $\text{Cu K}\alpha$ radiation ($\lambda = 1.54 \text{ \AA}$) at 40 kV and 30 mA. XPS analyses were operated on a Thermo ESCALAB 250 instrument. Specific surface area of composites was measured on a BET (NOVA 1000, Quanta Chrome,

America) under nitrogen atmosphere at 77 K. FE-SEM analyses were observed with a Hitachi S4800 FESEM at an accelerating voltage of 15 kV. TEM analyses were taken with a JEOL JEM-2100 microscope.

The electrochemical properties of the composite were investigated on a CHI660D electrochemical workstation (Shanghai, China) with conventional three-electrode system at room temperature. To prepare the working electrodes, the polytetrafluoroethylene with acetylene black (15 wt%) in ethylene solution were added to as-prepared composites to produce a homogeneous paste before pressed onto nickel foam current collectors. The electrodes were then dried under vacuum at 60°C for 24 h. The electrochemical performance of composites was investigated with standard CV, galvanostatic charge-discharge and EIS technique in 1 M Na_2SO_4 solution. CV measurements were performed in voltage ranging from 0 V to 0.8 V at a scan rate of 10, 30, 50 and 100 mV/s, respectively. Charge-discharge processes were carried out galvanostatically at 0.25~4 A/g current density in 0~1 V voltage range.

1. Stoller, M. D., Park, S. J., Zhu, Y., An, J. & Ruoff, R. S. Graphene-based ultracapacitors. *Nano Lett.* **8**, 3498–3502 (2008).
2. Burke, A. Ultracapacitors: why, how, and where is the technology. *J. Power Sources* **91**, 37–50 (2000).
3. Winter, M. & Brodd, R. J. What are batteries, fuel cells, and supercapacitors? *Chem. Rev.* **104**, 4245–4270 (2004).
4. Simon, P. & Gogotsi, Y. Materials for electrochemical capacitors. *Nat. Mater.* **7**, 845–854 (2008).
5. Liu, C., Li, F., Ma, L. & Cheng, H. Advanced materials for energy storage. *Adv. Mater.* **22**, E28–E62 (2010).
6. Fan, Z. *et al.* Asymmetric supercapacitors based on graphene/ MnO_2 and activated carbon nanofiber electrodes with high power and energy density. *Adv. Funct. Mater.* **21**, 2366–2375 (2011).
7. Wei, T. *et al.* A cost-effective supercapacitor material of ultrahigh specific capacitances: spinel nickel cobaltite aerogels from an epoxide-driven sol-gel process. *Adv. Mater.* **22**, 347–351 (2012).
8. Jiang, J. *et al.* Recent advances in metal oxide-based electrode architecture design for electrochemical energy storage. *Adv. Mater.* **24**, 5166–5180 (2012).
9. Si, P., Ding, S., Lou, X.-W. & Kim, D.-H. An electrochemically formed three-dimensional structure of polypyrrole/graphene nanoplatelets for high-performance supercapacitors. *RSC Adv.* **1**, 1271–1278 (2011).
10. Yuan, C. *et al.* Flexible hybrid paper made of monolayer Co_3O_4 microsphere arrays on rGO/CNTs and their application in electrochemical capacitors. *Adv. Funct. Mater.* **22**, 2560–2566 (2012).
11. Chang, J., Lin, C. T. & Tsai, W. T. Manganese oxide/carbon composite electrodes for electrochemical capacitors. *Electrochem. Commun.* **6**, 666–671 (2004).
12. Zheng, J., Cygan, P. J. & Jow, T. R. Hydrous ruthenium oxide as an electrode material for electrochemical capacitors. *J. Electrochem. Soc.* **142**, 2699–2703 (1995).
13. Zhang, J. *et al.* Template synthesis of tubular ruthenium oxides for supercapacitor applications. *J. Phys. Chem. C* **114**, 13608–13613 (2010).
14. Wu, Z. *et al.* High-energy MnO_2 nanowire/graphene and graphene asymmetric electrochemical capacitors. *ACS Nano* **4**, 5835–5842 (2010).
15. Wang, D., Li, F. & Cheng, H. Hierarchical porous nickel oxide and carbon as electrode materials for asymmetric supercapacitor. *J. Power Sources* **185**, 1563–1568 (2008).
16. Pang, S., Anderson, M. A. & Chapman, T. W. Novel electrode materials for thin-film ultracapacitors: comparison of electrochemical properties of sol-gel-derived and electrodeposited manganese dioxide. *J. Electrochem. Soc.* **147**, 444–450 (2000).
17. Cheng, F., Chen, J., Gou, X. & Shen, P. High-power alkaline Zn- MnO_2 batteries using γ - MnO_2 nanowires/nanotubes and electrolytic zinc powder. *Adv. Mater.* **17**, 2753–2756 (2005).



18. Yan, J. *et al.* Fast and reversible surface redox reaction of graphene-MnO₂ composites as supercapacitor electrodes. *Carbon* **48**, 3825–3833 (2010).
19. Ma, R., Bando, Y., Zhang, L. & Sasaki, T. Layered MnO₂ nanobelts: hydrothermal synthesis and electrochemical measurements. *Adv. Mater.* **16**, 918–922 (2004).
20. Bordjiba, T. & Belanger, D. Direct redox deposition of manganese oxide on multiscaled carbon nanotube/microfiber carbon electrode for electrochemical capacitor. *J. Electrochem. Soc.* **156**, A378–A384 (2009).
21. Bordjiba, T. & Belanger, D. Development of new nanocomposite based on nanosized-manganese oxide and carbon nanotubes for high performance electrochemical capacitors. *Electrochim. Acta* **55**, 3428–3433 (2010).
22. Ma, S. *et al.* Electrochemical properties of manganese oxide coated onto carbon nanotubes for energy-storage applications. *J. Power Sources* **178**, 483–489 (2008).
23. Dong, X. *et al.* MnO₂-embedded-in-mesoporous-carbon-wall structure for use as electrochemical capacitors. *J. Phys. Chem. B* **110**, 3019–6015 (2006).
24. Qian, Q., Lu, S. & Gao, F. Preparation of MnO₂/graphene composite as electrode material for supercapacitors. *J. Mater. Sci.* **46**, 3517–3522 (2011).
25. Yan, J. *et al.* Fast and reversible surface redox reaction of graphene-MnO₂ composites as supercapacitor electrodes. *Carbon* **48**, 3825–3933 (2010).
26. Jiang, H., Ma, J. & Li, C. Polyaniline-MnO₂ coaxial nanofiber with hierarchical structure for high-performance supercapacitors. *J. Mater. Chem.* **22**, 16939–16942 (2012).
27. Wang, J., Yang, Y., Huang, Z. & Kang, F. Rational synthesis of MnO₂/conducting polypyrrole@carbon nanofiber triaxial nano-cables for high-performance supercapacitors. *J. Mater. Chem.* **22**, 16943–16949 (2012).
28. Yu, G. *et al.* Enhancing the supercapacitor performance of graphene/MnO₂ nanostructured electrodes by conductive wrapping. *Nano Lett.* **11**, 4438–4442 (2011).
29. Yu, G. *et al.* Solution-processed graphene/MnO₂ nanostructured textiles for high-performance electrochemical capacitors. *Nano Lett.* **11**, 2905–2911 (2011).
30. Wang, G., Tang, Q., Bao, H., Li, X. & Wang, G. Synthesis of hierarchical sulfonated graphene/MnO₂/polyaniline ternary composite and its improved electrochemical performance. *J. Power Sources* **241**, 231–238 (2013).
31. Hou, Y., Cheng, Y., Hobson, T. & Liu, J. Design and synthesis of hierarchical MnO₂ nanospheres/carbon nanotubes/conducting polymer ternary composite for high performance electrochemical electrodes. *Nano Lett.* **10**, 2727–2733 (2010).
32. Wang, H., Bian, L., Zhou, P., Tang, J. & Tang, W. Core-sheath structured bacterial cellulose/polypyrrole nanocomposites with excellent conductivity as supercapacitors. *J. Mater. Chem. A* **1**, 578–584 (2013).
33. Wang, H. *et al.* Bacterial cellulose nanofiber-supported polyaniline nanocomposites with flake-shaped morphology as supercapacitor electrodes. *J. Phys. Chem. C* **116**, 13013–13019 (2012).
34. Novoselov, K. *et al.* Electric field effect in atomically thin carbon films. *Science* **306**, 666–669 (2004).
35. Lee, C., Wei, X., Kysar, J. & Hone, J. Measurement of the elastic properties and intrinsic strength of monolayer graphene. *Science* **321**, 385–388 (2008).
36. Park, S. & Ruoff, R. Chemical methods for the production of graphenes. *Nat. Nanotechnol.* **4**, 217–224 (2009).
37. Compton, O. & Nguyen, S. Graphene oxide, highly reduced graphene oxide, and graphene: versatile building blocks for carbon-based materials. *Small* **6**, 711–723 (2010).
38. Ma, S., Ahn, K., Lee, E., Oh, K. & Kim, K. Synthesis and characterization of manganese dioxide spontaneously coated on carbon nanotubes. *Carbon* **45**, 375–382 (2007).
39. Liu, Y. *et al.* Graphene/polypyrrole intercalating nanocomposites as supercapacitors electrode. *Electrochim. Acta* **112**, 44–52 (2013).
40. Li, Q., Zhang, C., Xue, Z. & Li, J. Preparation and characterization of polypyrrole microbelt via cotton template. *J. Chin. J. Chem. Phys.* **23**, 207–210 (2010).
41. Fu, X., Feng, J., Wang, H. & Ng, K. M. Room temperature synthesis of a novel γ -MnO₂ hollow structure for aerobic oxidation of benzyl alcohol. *Nanotechnology* **20**, 375601 (2009).
42. Yang, H. & Zeng, H. Preparation of hollow anatase TiO₂ nanospheres via ostwald ripening. *J. Phys. Chem. B* **108**, 3492–3495 (2004).
43. Gao, T. *et al.* Microstructures and Spectroscopic Properties of Cryptomelane-type Manganese Dioxide Nanofibers. *J. Phys. Chem. C* **112**, 13134–13140 (2008).
44. Liu, Z., Ma, R., Ebina, Y., Takada, K. & Sasaki, T. Synthesis and delamination of layered manganese oxide nanobelts. *Chem. Mater.* **19**, 6504–6512 (2007).
45. Zhu, C., Guo, S., Fang, Y., Han, L. & Wang, S. One-step electrochemical approach to the synthesis of graphene/MnO₂ nanowall hybrids. *Nano Res.* **4**, 648–657 (2011).
46. Zhu, J. & He, J. Facile synthesis of graphene-wrapped honeycomb MnO₂ nanospheres and their application in supercapacitors. *ACS Appl. Mater. Interfaces.* **4**, 1770–1776 (2012).
47. Nian, Y. R. & Heng, H. Nitric acid modification of activated carbon electrodes for improvement of electrochemical capacitance. *J. Electrochem. Soc.* **149**, A1008–A1014 (2002).
48. Han, G. *et al.* Sandwich-structured MnO₂/polypyrrole/reduced graphene oxide hybrid composites for high performance supercapacitors. *RSC Adv.* **4**, 9898–9904 (2014).

Acknowledgments

This research project was financially supported by the National Natural Science Foundation of China (Grant No. 21074055), Program for New Century Excellent Talents in University (NCET-12-0633), Jiangsu Province Natural Science Fund for Distinguished Young scholars (BK20130032), Doctoral Fund of Ministry of Education of China (No. 20103219120008), and the Fundamental Research Funds for the Central Universities (30920130111006).

Author contributions

T.W. conceived the work. H.G., Z.L., L.Y. and Z.S. performed the experiments. H.G., K.E., T.J. and T.W. analyzed the data and prepared the manuscript.

Additional information

Competing financial interests: The authors declare no competing financial interests.

How to cite this article: Han, G.Q. *et al.* MnO₂ Nanorods Intercalating Graphene Oxide/ Polyaniline Ternary Composites for Robust High-Performance Supercapacitors. *Sci. Rep.* **4**, 4824; DOI:10.1038/srep04824 (2014).



This work is licensed under a Creative Commons Attribution-NonCommercial-NoDerivs 3.0 Unported License. The images in this article are included in the article's Creative Commons license, unless indicated otherwise in the image credit; if the image is not included under the Creative Commons license, users will need to obtain permission from the license holder in order to reproduce the image. To view a copy of this license, visit <http://creativecommons.org/licenses/by-nc-nd/3.0/>